Repeatability Modeling for Wind-Tunnel Measurements: Results for Three Langley Facilities

Michael J. Hemsch*
Consultant, Williamsburg, VA 23188
Heather P. Houlden†
ViGYAN, Inc., Hampton, VA, 23666

Data from extensive check standard tests of seven measurement processes in three NASA Langley Research Center wind tunnels are statistically analyzed to test a simple model previously presented in 2000 for characterizing short-term, within-test and across-test repeatability. The analysis is intended to support process improvement and development of uncertainty models for the measurements. The analysis suggests that the repeatability can be estimated adequately as a function of only the test section dynamic pressure over a two-orders-of-magnitude dynamic pressure range. As expected for low instrument loading, short-term coefficient repeatability is determined by the resolution of the instrument alone (air off). However, as previously pointed out, for the highest dynamic pressure range the coefficient repeatability appears to be independent of dynamic pressure, thus presenting a lower floor for the standard deviation for all three time frames. The simple repeatability model is shown to be adequate for all of the cases presented and for all three time frames.

Nomenclature

14x22	LaRC 14- by 22-Foot Subsonic Tunnel
A	coefficient in model equation for instrument effective resolution
AT	across-test (variation of check standard test grand averages from test to test)
B	coefficient in model equation for standard deviation floor
C	general force or pressure coefficient
C_A	axial-force coefficient
C_L	lift coefficient
C_N	normal-force coefficient
CSM	check standard model
CSP	check standard probe
C'	calibration coefficient for the 14x22, DPC/DPI
d_4	bias correction factor for converting the median range to an estimate of the population standard deviation (Ref. 1)
DOF	number of degrees of freedom
DPC	14x22 calibration probe differential pressure; $p_{total} - p_{static}$, psf
DPI	14x22 test section reference differential pressure; $p_{total} - p_{static}$, psf
LaRC	Langley Research Center
LTPT	LaRC Low-Turbulence Pressure Tunnel
mR_{AT}	moving range of within-test grand averages
$\widetilde{mR}_{AT}$	median of the moving ranges in a control chart of the within-test grand averages for a canonical test condition
NTF	National Transonic Facility
q_∞	free-stream dynamic pressure, psf or psi

* Consultant, 234 Par Drive, Associate Fellow.
† Senior Aerospace Engineer, 30 Research Drive, Senior Member.

R_{WG}	range of the values within a group
$\tilde{R}_{WG}$	median of the R_{WG} in a control chart for a canonical test condition
R_{WT}	range of the group averages within a test
$\tilde{R}_{WT}$	median of the R_{WT} in a control chart for a canonical test condition
S	sample standard deviation
S_{ref}	reference area for force and moment coefficients
WT	within-test (variation of check standard group averages within a test)
WG	within-group (variation of a single check standard measurement within a group, i.e. back-to-back)
ρ	correlation coefficient
σ	population standard deviation
$\hat{\sigma}$	estimate of the population standard deviation based on pooled samples
$\sigma_{C,AT}$	additional repeatability to be RMS added to $\sigma_{C,WG}$ and $\sigma_{C,WT}$ for across-test measurements of coefficient C
$\sigma_{C,WG}$	repeatability to be expected for C for short-term measurements; i.e. back-to-back
$\sigma_{C,WT}$	additional repeatability to be RMS added to $\sigma_{C,WG}$ for within-test measurements of coefficient C
$\hat{\sigma}_{AT}$	estimate of the repeatability standard deviation of the within-test coefficient grand averages; see Eq.(4)
$\hat{\sigma}_{WT}$	estimate of the repeatability standard deviation of the within-test coefficient group averages; see Eq.(3)
$\hat{\sigma}_{WG}$	estimate of the repeatability standard deviation of the within-group coefficient values; see Eq.(2)

Introduction

In 1998, the NASA Langley Research Center (LaRC) began a campaign of check standard testing in most of its major wind tunnels. The purpose of check standard testing is to track the behavior of a wind tunnel's measurement systems over time, including the short-term, within-test and across-test time frames. This is done using an artifact that is stable over time to provide a load on a measurement system. The actual load is not important, as long as it is steady, since it serves only to measure the instrument variation over time. The artifact should also not introduce variation that is not associated with the measurement process, e.g. unsteady flow. Typical artifacts used at LaRC are (1) wind tunnel models that are set aside for check standard testing only, (2) select pitot-static probes used to measure the test section conditions, and (3) chord-wise rows of pressures on wings. Statistical process control charts[1, 2] have been developed for carrying out the tracking and serve as an early warning system of potential problems with the measurement processes. Preliminary analyses of the early LaRC check standard results were presented in References 3-5, together with a fuller description of the check standard process. The early results for the short-term time frame suggested a simple model for correlating the results across the entire dynamic pressure range of a given facility.

The model proposed in References 3-5 was developed by carrying out the error propagation equation[6] for a typical force or pressure coefficient as shown in Appendix A. The result is[‡]

$$\hat{\sigma} = \sqrt{\left(\frac{A}{q_\infty}\right)^2 - 2\rho\left(\frac{A}{q_\infty}\right)B + B^2} \tag{1}$$

where $\hat{\sigma}$ is the model estimate of the population standard deviation, A is the effective resolution of the instrument(s) divided by the reference area, q_∞ is the dynamic pressure in the test section, B is the coefficient of variation of the dynamic pressure $\left(\sigma_{q_\infty} / q_\infty\right)$ multiplied by the force or pressure coefficient value, and ρ is the correlation coefficient[6] for the A / q_∞ and B sources of variation.

[‡] For the 14x22 analyses, q_∞ is replaced by DPI.

The purpose of this work is to test that model for the three time frames using extensive check standard tests for seven measurement processes in three LaRC tunnels. This kind of statistical testing for standard deviation models is hampered by the need for a fairly large number of degrees of freedom (DOF) to keep the confidence limits reasonable for prediction. As shown[§] in Figure 1, for example, it is necessary to obtain 20 DOF in order to limit the scatter to ±50% of the population value. Of course, the population standard deviation is unknown except through the taking of samples which, by necessity, have a small DOF at any given time. Fortunately for this work, regular check standard testing will eventually produce sufficient DOF with which to model the three time frames of variation. The three time frames to be dealt with in this paper and the methods for estimating the corresponding standard deviations are (1) the short-term variation of the coefficient (C) within a group (pooled over the tests), σ_{WG} ; (2) the variation of group averages within a test (pooled over the tests), σ_{WT} ; (3) the variation of the within-test grand averages, σ_{AT} . For the model testing herein, the estimates of the population standard deviations are given by[1]:

Within-Group (WG):

$$\hat{\sigma}_{WG} = \tilde{R}_{WG} / d_4 \tag{2}$$

which reads "the estimate of the within-group population standard deviation is equal to the median of all of the within-group ranges divided by the bias correction factor d_4".

Within-Test (WT):

$$\hat{\sigma}_{WT} = \tilde{R}_{WT} / d_4 \tag{3}$$

which reads "the estimate of the population standard deviation of group averages obtained within a test is equal to the median of all of the within-test group average ranges divided by the bias correction factor d_4".

Across-Test (WT):

$$\hat{\sigma}_{AT} = \widetilde{mR}_{AT} / d_4 \tag{4}$$

which reads as "the estimate of the population standard deviation of within-test grand averages obtained within a test is equal to the median moving range of all of the within-test grand averages divided by the bias correction factor d_4". The bias correction factor, d_4, for Eq.(2-4) is a function of the DOF.[1]

Example results will be presented below for

1. The test section calibration coefficient (C') of the 14x22 measured by the check standard probe (CSP)
2. The normal-force coefficient (C_N) measured on the 14x22 check standard model (CSM)
3. The axial-force coefficient (C_A) measured on the 14x22 CSM
4. The normal-force coefficient (C_N) measured on the NTF CSM
5. The axial-force coefficient (C_A) measured on the NTF CSM
6. The airfoil lift-coefficient (C_L) measured on the LTPT CSM using the main balance

[§] The control chart limits used in Figure 1 are given in Appendix VI of Ref. 2 for the *average* of the sample standard deviations. Medians are used instead throughout this analysis to make the control charts more robust to occasional outliers. Thus the limits in Figure 1 should be inflated somewhat for the approach herein. However, the authors have been unable to find limits tables for medians for large DOF. Hence, the values of Figure 1 are used herein, but with the caveat that they should be somewhat bigger.

7. The airfoil lift coefficient (C_L) measured on the LTPT CSM using a chord-wise row of pressure taps at mid-span.

The paper will conclude with some general observations about the results. It is beyond the scope of this effort to investigate the sources of the observed variations.

Case 1. 14x22 Check Standard Probe (Test Section Calibration Coefficient)

The 14x22 is a large atmospheric subsonic closed-return tunnel[7] that is used for a wide range of tests, including ground wind loads on launch vehicles, free-flight testing, helicopter performance and acoustic testing, and landing and takeoff performance. In 1996 the staff decided to use a new test section calibration model in which the calibration coefficient C' is a function of the test section reference pitot-static pressure difference, DPI. This new model significantly improved the accuracy of the calibration. C' is now defined as

$$C' = \frac{\left(p_{total} - p_{static}\right)_{probe}}{\left(p_{total} - p_{static}\right)_{reference}} = \frac{DPC}{DPI} \tag{5}$$

which means that two instruments are needed to measure C'. The performance of the two instruments used is assumed to be the same since they are identical. (See Appendix B for a derivation of the expected performance at very low test-section dynamic pressures.) The probe is mounted in the test section as shown in Figure 2. The probe head is located on the test section centerline at the most common center of rotation of the model mounting system. The test section can be configured in several different ways. For this case, the test section is closed, i.e. the walls, ceiling and floor enclose the space.

The C' measurements are obtained in a group defined as three back-to-back polars through the DPI range from 0.5 to 120 psf. The data are piece-wise linearly interpolated to the nominal DPI canonical conditions to avoid including set point error in the measurement variation. For each canonical condition, a robust measurement of the standard deviation was obtained using the control chart median ranges.[1] (See Eq. (2-4).) The group standard deviation is a measure of the short-term repeatability of the calibration measurement. Multiple groups were usually obtained in each test, which allowed measurement of the within-test variation using the variation of the group averages. Fourteen tests have been carried out so far, which allows measurement of the across-test variation using the grand averages of the within-test results. The standard deviations and grand averages are tracked over time using statistical process control charts for each canonical DPI test condition.[1, 2, 6]

Figure 3 shows a log-log plot of the three time frames of variation obtained using the medians from the control charts for each canonical condition. A log-log plot is used to emphasize the behavior in the low q_∞ region. In this region, the calibration coefficient standard deviations are expected to be proportional to $1/DPI$ (see Appendix B). The regions where σ is constant are also apparent for high DPI.

Figure 4(a) is a log-log plot showing the measured within-group repeatability standard deviations (symbols), together with the fitted model (red line) of Eq.(1) as a function of DPI. For the low Mach numbers in this tunnel, DPI is very close to q_∞. It is convenient for this tunnel to use DPI for the abscissa rather than q_∞ because DPI is used to set the conditions during the tests. The model coefficient, A, is obtained by averaging $\sigma * DPI$ over the region for which the $1/DPI$ dependence holds. The model coefficient, B, is obtained by averaging σ over the region where it seems to be constant (given the observed scatter). Finally, the correlation coefficient, ρ, is chosen to fit the largest number of points between the limits (to be discussed below).

The model coefficients are given in Table 1. Also shown in Figure 4(a) are upper and lower limits (grey lines) based on the estimated number of degrees of freedom (DOF) for the groups. (See Figure 1.) The results shown are for 45 groups with 3 measurements each. Thus, each group is estimated to contribute 2 DOF, yielding 90 DOF to date. The limits are control chart limits for 90 DOF placed on the model. The authors prefer to use control chart limits on the model rather than confidence limits placed on the data because they clearly show the range of sample standard deviation scatter to be expected by chance alone. For this case, all of the data are within or on the limits. Figure 4(a) also shows the result that would be expected for the two Mensor pressure sensors using the manufacturer's quoted

combined repeatability, nonlinearity and hysteresis (i.e. with $B = 0$). See Appendix B for the derivation. Figure 4(b) shows the same information using a semi-log plot to emphasis the region of constant σ that extends over the upper half of the test section DPI range.

Figures 5 and 6 show similar results for the variation of the group averages within a test and the variation of the test grand averages respectively across the available tests. Multiple groups were obtained in 11 of the 14 tests with an average of 3 groups each. With an estimated 2 DOF for each such test, the total number of DOF is 22. Since there have been a total of 14 tests, the number of DOF for the across-test variation is 13. It should be noted that the limits expand significantly as the number of DOF is reduced, i.e. 13 versus 22 versus 90. (See Figure 1.) Given the very large range of the limits for the across-test results, it would seem reasonable to consider the fit provisional rather than confirmed.

Figure 7 compares the models for the three time frames on a log-log plot, showing that the variations for the longer time frames are dominant. Note that $\hat{\sigma}_{WT}$ is roughly 3 times larger than $\hat{\sigma}_{WG}$ for the larger values of DPI. For the same DPI range, $\hat{\sigma}_{AT}$ is almost three times $\hat{\sigma}_{WT}$. The model coefficients are given in Table 1. Appendix C presents the necessary equations for extracting the repeatability that a customer would expect to see for a single C' measurement within or across tests.

Case 2. 14x22 Check Standard Model (Normal-Force Coefficient)
The check standard model for the 14x22 is the elliptical wing shown in Figure 8. It is tested in a fashion similar to that of the CSP except that three back-to-back polars are obtained for each canonical DPI condition. The groups are formed after interpolating the data to the nominal angle-of-attack (AOA) set points. Only the data at an AOA of two degrees are used in the current analysis. This is the AOA that is expected to give the smoothest flow over the model. Since the instrument used for the CSM testing is multi-component (normal, axial and side forces and pitch, yaw and roll moments), the measurements for the purposes of check standard testing are taken about the balance electrical center to avoid combining the individual measurements (to first order).[**]

The results from the control chart medians for the normal-force coefficient variation are shown in Figures 9-11 for all three time frames. Figure 9 shows the control chart medians for the within-group results, together with the model fit and the limits for the 41 groups (82 DOF). Also shown is the expected behavior if the resolution of the balance at 1σ were 0.012% of full-scale (with $B = 0$). That value is roughly what one would expect for the resolution of LaRC single element balances. Note that the control limits about the model fit contain all of the measured results. Similar results are shown in Figures 10 and 11 for the within-test (11 tests with multiple groups, 22 DOF) and across-test (13 tests, 12 DOF) variations respectively. Again, all of the data are contained within the control limits about the model fit. Although the limits are fairly wide for the across-test results, the fit looks reasonably confirmed.

The three model fits are shown together in Figure 12. It is apparent that the across-test variation is only significant for DPI ≥ 15 psf. The model fit coefficients are given in Table 1.

Case 3. 14x22 Check Standard Model (Axial-Force Coefficient)
The results from the control chart medians for the axial-force coefficient variation are similar to those for the normal-force coefficient and are shown in Figures 13-15 for all three time frames. Figure 13 shows the within-group results, together with the model fit and the limits for the 41 groups (82 DOF). Also shown is the expected behavior if the resolution of the balance at 1σ were 0.012% of full-scale (with $B = 0$). Note that the control limits about the model fit contain all of the measured results. Similar results are shown in Figures 14 and 15 for the within-test and across-test variations respectively. Again, all of the data are contained within the control limits about the model fit. And again, although the limits are fairly wide for the across-test results, the fit looks reasonably confirmed.

The three model fits are shown together in Figure 16. It is apparent that the across-test variation is only significant for the very highest portion of the DPI range. The model fit coefficients are given in Table 1. It is interesting to note that the correlation coefficients for the three time frames match those for the C_N variation.

[**] It is impossible to separate the second-order effects from the measurements due to the complex second-order 6-component calibration matrix used to reduce the data to engineering units.

Case 4. NTF Check Standard Model (Normal-Force Coefficient)
The check standard model for the NTF is the Pathfinder I as described in Reference 8 and shown in Figure 17. The NTF is a transonic pressure tunnel that can be run with warm air or with cryogenic nitrogen. Because of the large costs associated with cryogenic testing, the check standard testing is done in air with occasional cryogenic testing to augment those results. Also, because the NTF is a pressure tunnel (total pressure range from 1 to 10 atmospheres), a more than two-orders of magnitude range of q_∞ is available for model testing.

Analysis of the normal-force coefficient data from the NTF check standard testing is identical to that shown in the three previous examples. The σ for the three time frames are shown in Figures 18-20 with the control limits. The NTF check standard testing is not always conducted at each of the canonical conditions. Hence, the DOF for the various canonical conditions do not have the same values and the control limits are shown as individual "error bars" on the model fits (for the appropriate DOF). Also, shown in Figure 18 is the observed effective resolution of the normal-force measurement process (black line) (with $B = 0$). As before with the 14x22 instrument processes, the resolution is roughly what would be expected for an NTF single element balance.

The control limits do not capture all of the data for the three time frames. For the within-group variation there are three points each outside the limits. The within- and across-test fits have one point each outside the limits. The across-test DOF for 15, 34 and 2400 psf are small leading to lower limits of zero. The model fits for the three time frames are shown in summary in Figure 21. The across-test variation is clearly dominant. The model fit coefficients are given in Table 1.

Case 5. NTF Check Standard Model (Axial-Force Coefficient)
Analysis of the axial-force coefficient data from the NTF check standard testing is identical to that shown in the four previous examples. The σ for the three time frames are shown in Figures 22-24 with the control limits. Also, shown in Figure 22 is the observed effective resolution of the axial-force measurement process (black line with $B = 0$). The resolution of the NTF CSM balance axial measurement is roughly what would be expected.

The control limits do not capture all of the data for the within-group and within-test time frames. For within-group data, there are two points outside the limits. For the within-test fit, there are three points outside the limits. The model fits for the three time frames are shown in summary in Figure 25. The across-test variation is clearly dominant. The model fit coefficients are given in Table 1. It is interesting to note the similarity of the normal- and axial-force coefficient fits in Figures 21 and 25 respectively.

Cases 6 and 7. LTPT Check Standard Model Lift Coefficient Measured by Two Systems
The check standard model for the LTPT is a single element airfoil as shown in cross-section in Figure 26, together with the location of a chordwise ring of pressure taps. The LTPT test section is three feet wide and seven feet high and the airfoil chord is two feet long. Although check standard testing was not conducted after the first two tests, those two tests provided an interesting set of lift coefficient (C_L) data with which to determine and compare the repeatability of the main balance and integrated pressure measurement systems. The data were obtained in multiple groups of 10 back-to-back polars. The analysis is performed only at the design AOA points (2 degrees) after interpolation to avoid set point error. (The lift coefficient is roughly 0.7 at the design angle of attack.) The Mach number was 0.2 for the range[††] $0.4 \le q_\infty \le 4.0$. To obtain data for the range $0.05 \le q_\infty \le 0.4$ the Mach number was decreased accordingly.

The main balance within-group results are shown in Figure 27 with the integrated pressure results shown in Figure 28. The models fit is shown with the control limits for each canonical condition[‡‡]. The model fit coefficients are given in Table 1. For the balance data, four out of the seven points are at the edge of the control limits. For the integrated pressure data, one point is at a control limit. There were too few within-test results to be able to test a model for that time frame.

[††] The LTPT can be pressurized to 10 atm, providing a 10-fold range of q_∞ at a given Mach number.

[‡‡] Different numbers of groups were obtained at the various canonical q_∞ test conditions. Hence, the control limits are shown as "error" bars on the model fits.

The model fits for the two measurement processes are compared in Figure 29. While the pressure measurement system was designed to give considerably better results than those from the main balance at low q_∞, it was a bit surprising that the two processes would appear to converge to the same repeatability for the highest q_∞. This result may lend more credibility to the provisional model of Eq. (1) since the model suggests that the repeatability floor is independent of the force or pressure measurement process used. But it must be stressed that this possibility must remain conjecture until high DOF results are obtained with two or more measurement systems measuring the same thing in the same tunnel.

Concluding Observations

With the seven examples given above, the following observations seem reasonable:

1. The repeatability model appears to work for all three time frames of variation; although, when the limits are wide, the agreement should be considered provisional.
2. The within-group variation for low q_∞ is clearly due to the known resolution of the measurement system for the six example cases for which the information is available. (The resolution of the integrated pressure measurement of lift is not known.)
3. The within-group variation for higher q_∞ may be independent of the measurement system used. (See LTPT example.) But extensive (high DOF) additional testing would be required to determine if this possible result holds for the within-test and across-test variation,
4. For 4 out of the 17 model fits the correlation coefficient is one or nearly one (probe within-test, elliptical wing within-test for C_N, C_A, airfoil balance within-group). For the other 13 fits, the correlation coefficient would usually be considered statistically insignificant, although it is certainly needed here to make the model work in the transition regions.
5. The within-test and across-test variation at both low and high q_∞ seem unreasonably large relative to the within-group variation and significant performance improvement might be possible by examining the measurement process in detail.
6. Since the measurement of q_∞ may be the dominant source of variation for coefficients obtained at high q_∞ values, performance improvement might be possible by changing the measurement process. Currently, the time constants for the balance and dynamic pressure systems are very different in all of the tunnels.

Finally, using a rational (mechanistic) model with which to fit the data is, in a sense, equivalent to pooling the data (increasingly the DOF) over the whole test condition range. Hence, the model itself is likely to be known more accurately than the individual values at the various conditions.

Acknowledgements

The authors gratefully thank the staffs of the LTPT, 14x22 and NTF for acquiring and allowing the authors to use the check standard results presented in the analysis. This work was partially funded by NASA Contract NNL04AA03B.

References

1. Wheeler, D. J., *Advanced Topics in Statistical Process Control*, SPC Press 1995.
2. Montgomery, D. C., *Introduction to Statistical Quality Control*, 3rd Edition, Wiley 1996.
3. Hemsch, M. J., Grubb, J. P., Krieger, W. B., Cler, D. L.,"Langley Wind Tunnel Data Quality Assurance --- Check Standard Results", AIAA-2000-2201, June 2000.
4. Hemsch, M. J., Tuttle, D. G., Houlden, H. P., Graham, A. B., "Measurement of Force Balance Repeatability and Reproducibility in the NTF", AIAA-2004-0771, January 2004.
5. Hemsch, M. J., "Analysis of Flow Angularity Repeatability Tests in the NTF", AIAA-2006-0518, January 2006.
6. Mandel, J., *The Statistical Analysis of Experimental Data*, Dover 1984.
7. Gentry, G. L., Quinto, P. F., Gatlin, G. M., Applin, Z. T., "The Langley 14- by 22-Foot Subsonic Tunnel: Description, Flow Characteristics and Guide for Users", NASA TP 3008, 1990.

8. Jacobs, P. F., Gloss, B. B., "Longitudinal Aerodynamic Characteristics of a Subsonic Energy Efficient Transport Configuration in the National Transonic Facility", NASA TP 2922, 1989.

Appendix A --- Derivation of Model Equation for Balance and Pressure Coefficients

Consider the coefficient

$$C = \frac{F}{q_\infty S_{ref}} \tag{A.1}$$

where F is the instrument output, q_∞ is the test section dynamic pressure and S is the reference area. Differentiating Eq.(A.1) to obtain the sensitivity coefficients for the variables F and q_∞ gives

$$\frac{\partial C}{\partial F} = \frac{1}{q_\infty S_{ref}} \tag{A.2}$$

$$\frac{\partial C}{\partial q_\infty} = -\frac{C}{q_\infty} \tag{A.3}$$

The error propagation equation is then given by[8]

$$\hat{\sigma}^2 = \left(\frac{1}{q_\infty S_{ref}}\right)^2 \sigma_F^2 + 2\rho\left(\frac{1}{q_\infty S_{ref}}\right)\left(-\frac{C}{q_\infty}\right)\sigma_F \sigma_{q_\infty} + \left(-\frac{C}{q_\infty}\right)^2 \sigma_{q_\infty}^2 \tag{A.4}$$

Let A and B be defined by

$$A = \frac{\sigma_F}{S_{ref}} \tag{A.5}$$

$$B = C\frac{\sigma_{q_\infty}}{q_\infty} \tag{A.6}$$

Then Eq.(A.4) becomes

$$\hat{\sigma} = \sqrt{\left(\frac{A}{q_\infty}\right)^2 - 2\rho\left(\frac{A}{q_\infty}\right)B + B^2} \tag{A.7}$$

which is the desired model equation.

Appendix B --- Derivation of 14x22 C' Check Standard Probe Measurement Resolution

By definition

$$C' = \frac{DPC}{DPI} \tag{B.1}$$

The sensitivities of C' with respect to the two measurements are given by

$$\frac{\partial C'}{\partial DPC} = \frac{1}{DPI} \tag{B.2}$$

and

$$\frac{\partial C'}{\partial DPI} = -\frac{C'}{DPI} \tag{B.3}$$

Combining the variances, assuming that they are uncorrelated (and small), gives

$$\sigma_{C'}^2 = \left(\frac{\partial C'}{\partial DPC}\right)^2 \sigma_{DPC}^2 + \left(\frac{\partial C'}{\partial DPI}\right)^2 \sigma_{DPI}^2 \tag{B.4}$$

Substituting Eqs.(B.2, B.3) into Eq.(B.4) and taking the square root gives

$$\sigma_{C'} = \frac{1}{DPI}\sqrt{\sigma_{DPC}^2 + \left(C'\sigma_{DPI}\right)^2} \tag{B.5}$$

Since the type and range of the two Mensor's are identical, we shall assume that $\sigma_{DPC} \cong \sigma_{DPI}$ so that Eq.(C.5) becomes

$$\sigma_{C'} \approx \frac{\sigma_{DPI}}{DPI}\sqrt{1 + C'^2} \tag{B.6}$$

It is known that $1.15 \le C' \le 1.18$ so that Eq.(C.6) is given by

$$\sigma_{C'} \approx 1.5\frac{\sigma_{DPI}}{DPI} \tag{B.7}$$

The full-range of the Mensors is 1 psi which are quoted to be accurate to 0.009% FS. If we assume that the quote is for 2-sigma, then the manufacturer's quote for combined nonlinearity, hysteresis and repeatability is

$$\sigma_{DPI} = (0.5)(144\ psf)(0.00009) = 0.00648\ psf \tag{B.8}$$

Substituting Eq.(B.8) into Eq.(B.7) gives

$$\sigma_{C'} \approx 1.5\frac{0.00648\ psf}{DPI} = \frac{0.00972\ psf}{DPI} \tag{B.9}$$

Appendix C --- Method for Combining Within-Group, Within-Test and Across-Test Results

By definition (see Nomenclature)

$$\sigma_{WT}^2 = \sigma_{C,WT}^2 + \frac{1}{n}\sigma_{WG}^2 \tag{C.1}$$

Rearranging Eq.(C.1) gives

$$\sigma_{C,WT}^2 = \sigma_{WT}^2 - \frac{1}{n}\sigma_{WG}^2 \tag{C.2}$$

Also by definition

$$\sigma_{AT}^2 = \sigma_{C,AT}^2 + \frac{1}{N}\sigma_{WT}^2 \tag{C.3}$$

Rearranging Eq.(C.3) gives

$$\sigma_{C,AT}^2 = \sigma_{AT}^2 - \frac{1}{N}\sigma_{WT}^2 \tag{C.4}$$

The result of interest for within-test repeatability of a single measurement of the coefficient is

$$\sigma_{C,WG+WT}^2 = \sigma_{WG}^2 + \sigma_{C,WT}^2 \tag{C.5}$$

Substituting Eq.(C.2) into Eq.(C.5) and rearranging gives the desired expression

$$\boxed{\sigma_{C,WG+WT}^2 = \left(1 - \frac{1}{n}\right)\sigma_{WG}^2 + \sigma_{WT}^2} \tag{C.6}$$

Similarly, the result of interest for across-test repeatability of a single measurement of the coefficient is

$$\sigma^2_{C,WG+WT+AT} = \sigma^2_{WG} + \sigma^2_{C,WT} + \sigma^2_{C,AT} \tag{C.7}$$

Substituting Eq.(C.2) and Eq.(C.4) into Eq.(C.7) and rearranging gives

$$\boxed{\sigma^2_{C,WG+WT+AT} = \left(1-\frac{1}{n}\right)\sigma^2_{WG} + \left(1-\frac{1}{N}\right)\sigma^2_{WT} + \sigma^2_{AT}} \tag{C.8}$$

Results from the fits in the Figures 7, 12, 16, 21 and 25 can be substituted into Eq.(C.6) and Eq.(C.8) for prediction purposes. For the cases in this paper, n is always equal to 3 and N is equal to 3 on the average.

Facility	Check Standard	Time Frame	A	B	ρ
14x22	Pitot-Static Probe	Back-to-Back q_∞ Sweeps	0.00985	0.000325	0.225
|	|	Within-Test	0.0109	0.000956	-0.9
|	|	Across-Test	0.0160	0.00267	-0.2
|	Elliptical Wing (CN)	Back-to-Back Polars	0.00919	0.000321	0.2
|	|	Within-Test	0.025	0.00067	-1
|	|	Across-Test	0.0163	0.00159	0
|	Elliptical Wing (CA)	Back-to-Back Polars	0.00266	0.000061	0.2
|	|	Within-Test	0.0050	0.00012	-1
|	|	Across-Test	0.0032	0.00014	0
NTF	Pathfinder I (CN)	Back-to-Back Polars	0.126	0.0009	0.2
|	|	Within-Test	0.40	0.00075	0.4
|	|	Across-Test	0.50	0.00143	0.22
|	Pathfinder I (CA)	Back-to-Back Polars	.0149	0.00005	0.2
|	|	Within-Test	0.0390	0.00006	0.3
|	|	Across-Test	0.0500	0.000235	0.22
LTPT	Efficient Airfoil (Balance)	Back-to-Back Polars	0.00306	0.0007	-1
|	Efficient Airfoil (Integrated Pressure)	|	0.000826	0.0012	0

Table 1. Model Coefficients

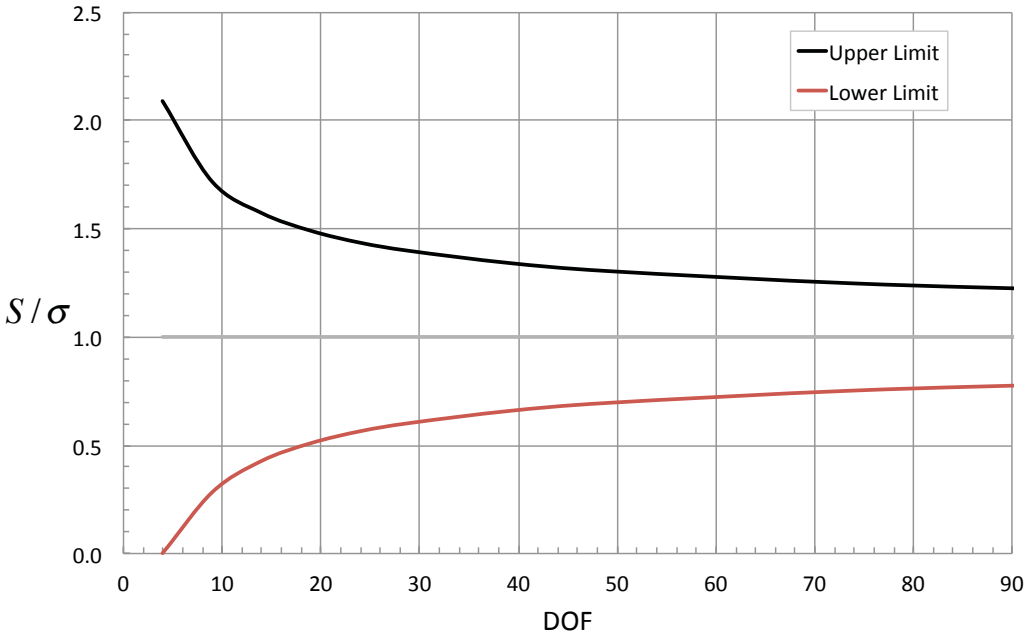

Figure 1. Control limits for samples of the standard deviation pooled by averaging (Ref. 2), normalized by the population standard deviation.

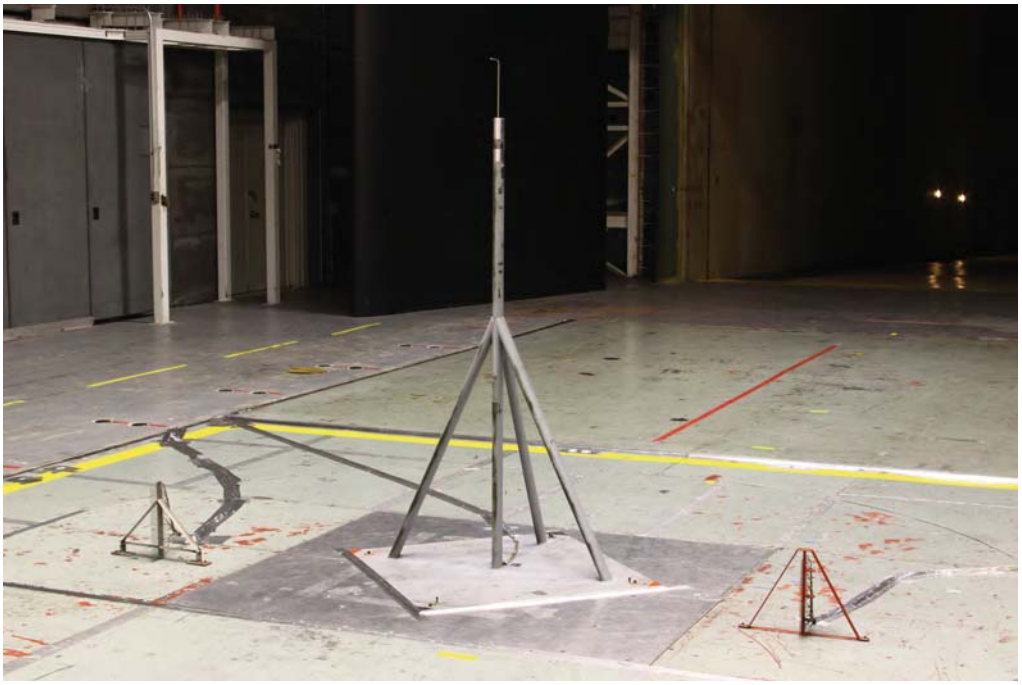

Figure 2. The 14- by 22-Foot Subsonic Tunnel check standard probe (CSP) on its stand in the test section.

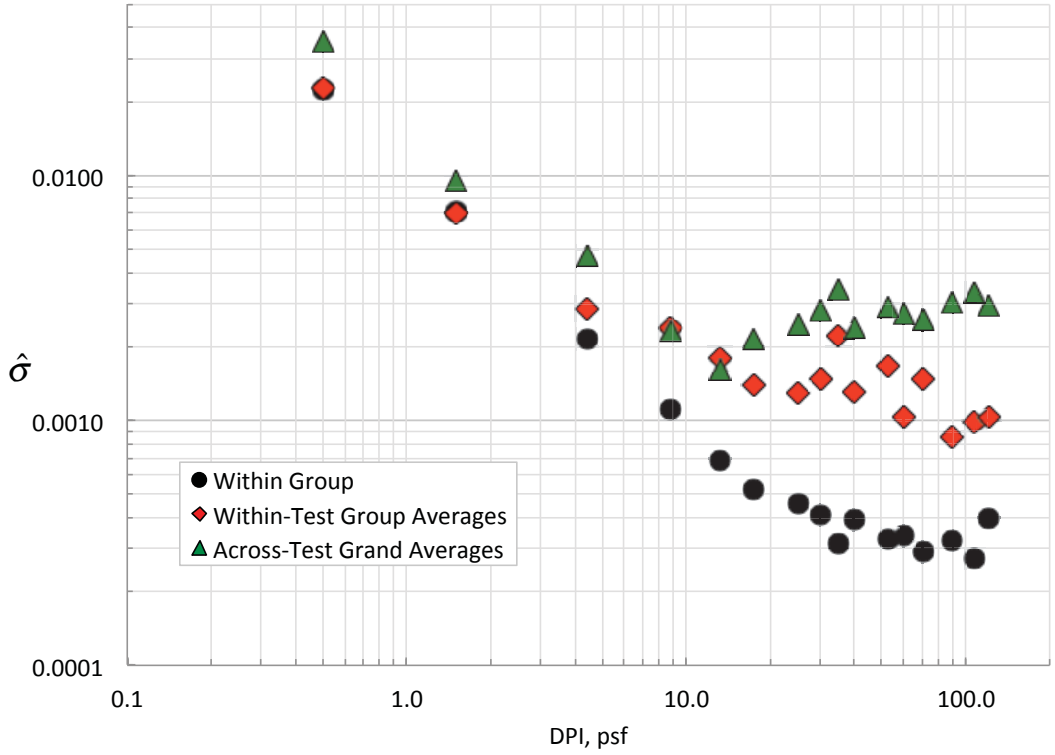

Figure 3. Log-log plot of variation of median $\hat{\sigma}$ for C' for the three time frames; 14x22 CSP.

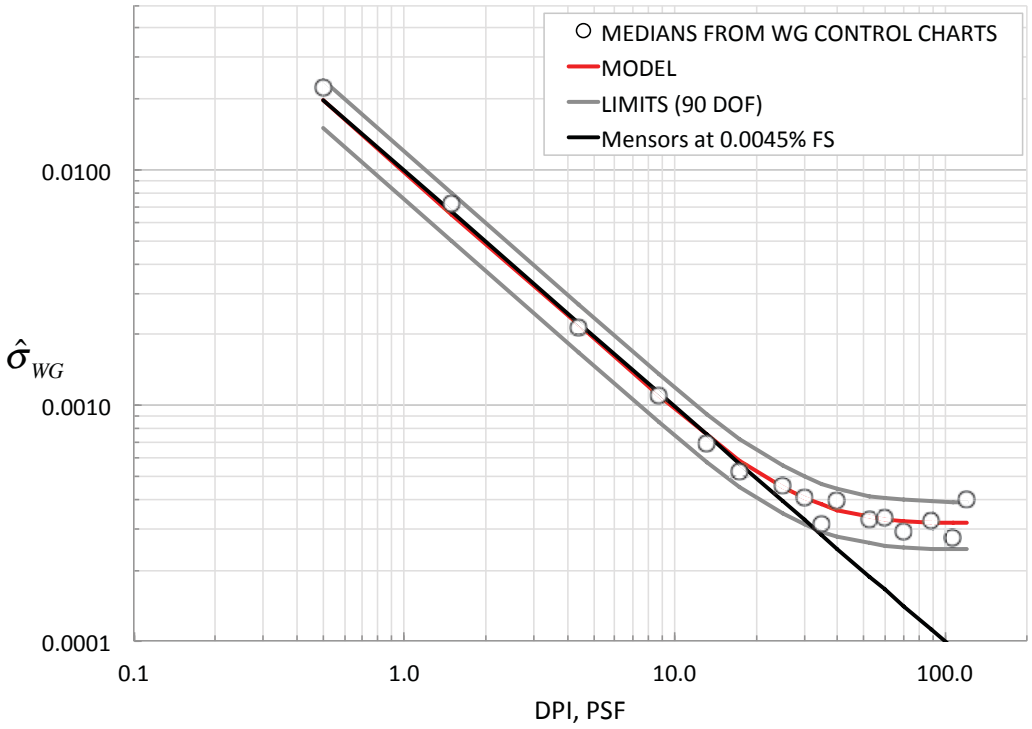

(a) Log-log plot

Figure 4. Model of $\hat{\sigma}_{WG}$ for C' with control limits for 90 DOF; 14x22 CSP.

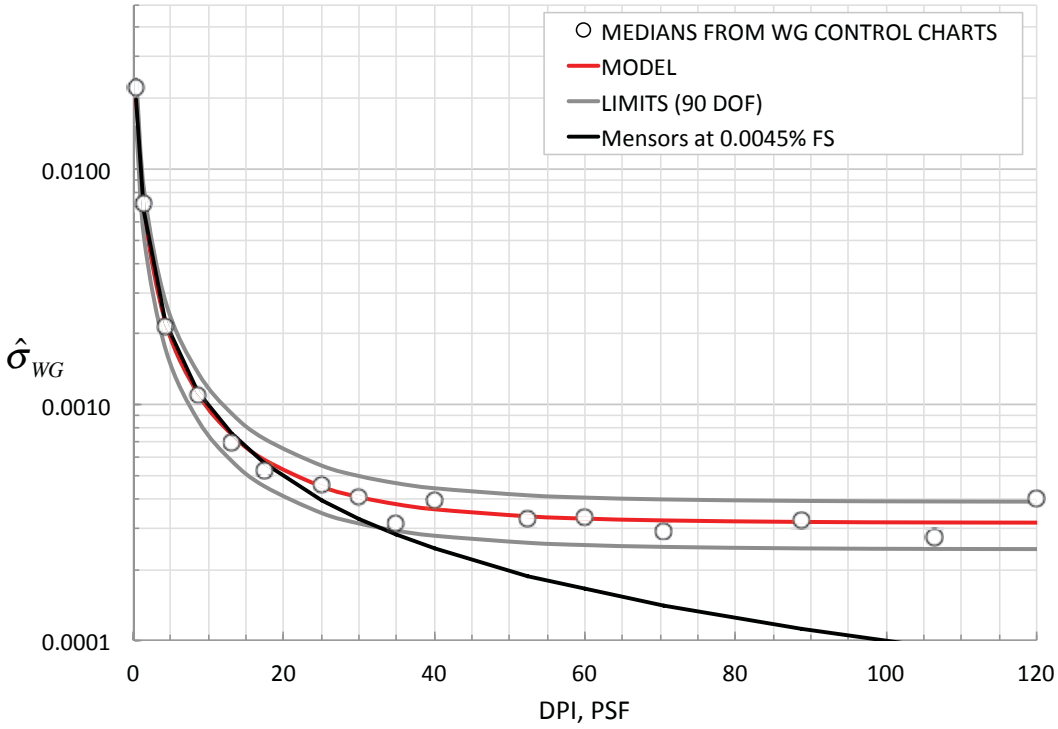

(b) Semi-log plot.

Figure 4. Concluded

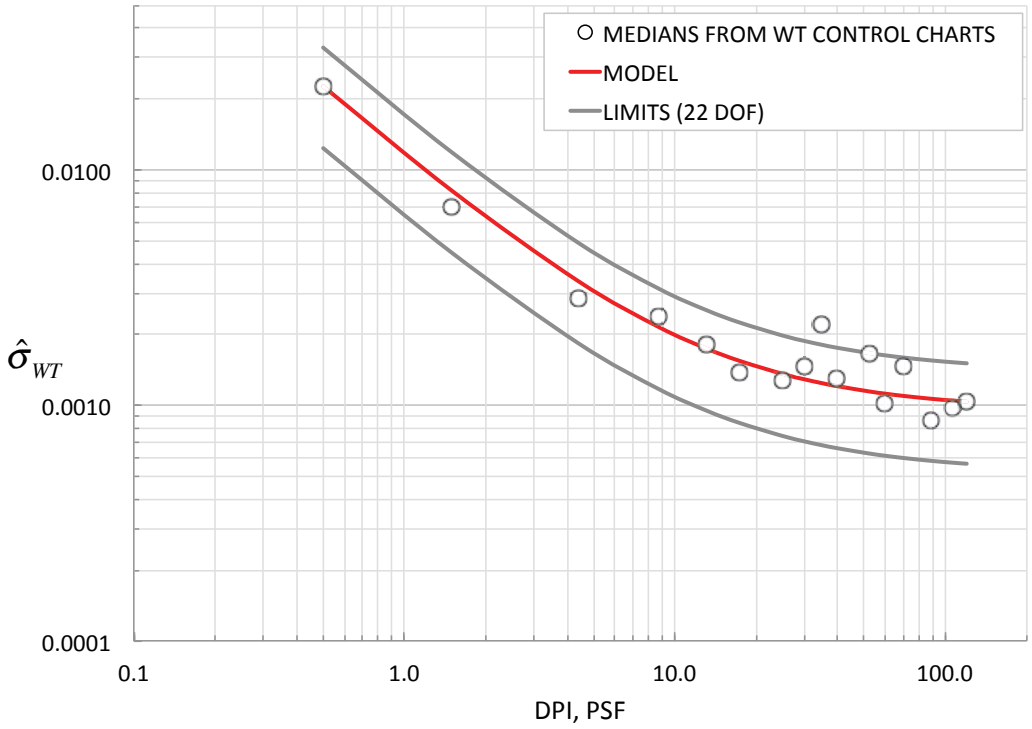

Figure 5. Model of $\hat{\sigma}_{WT}$ for C' with control limits for 22 DOF; 14x22 CSP.

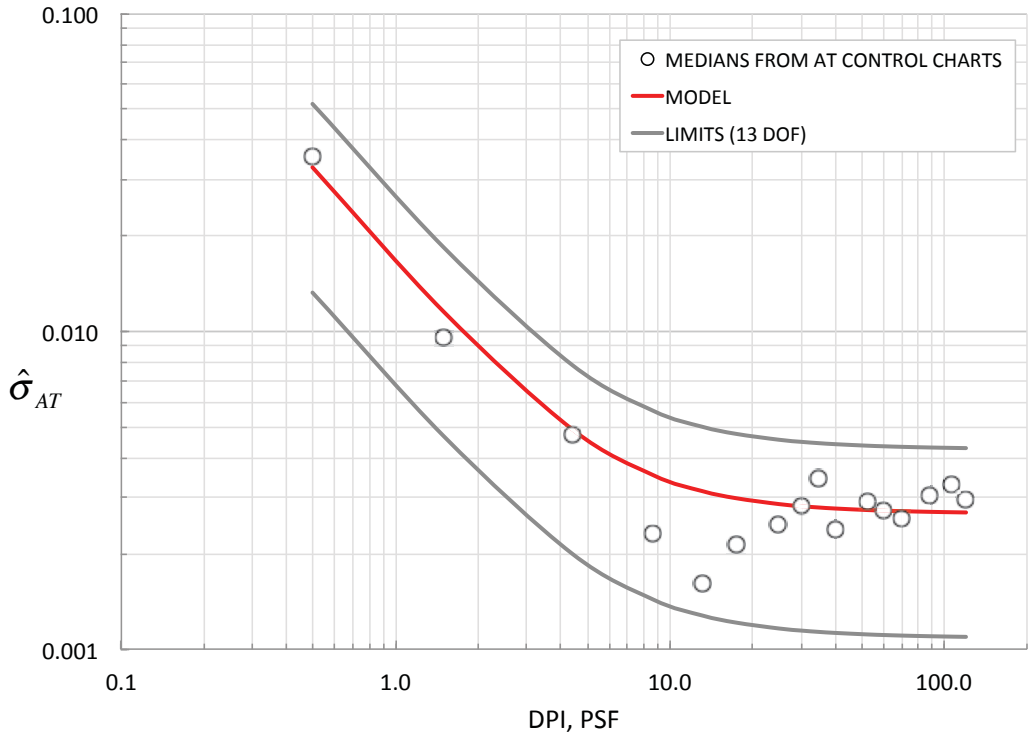

Figure 6. Model of $\hat{\sigma}_{AT}$ for C' with control limits for 13 DOF; 14x22 CSP.

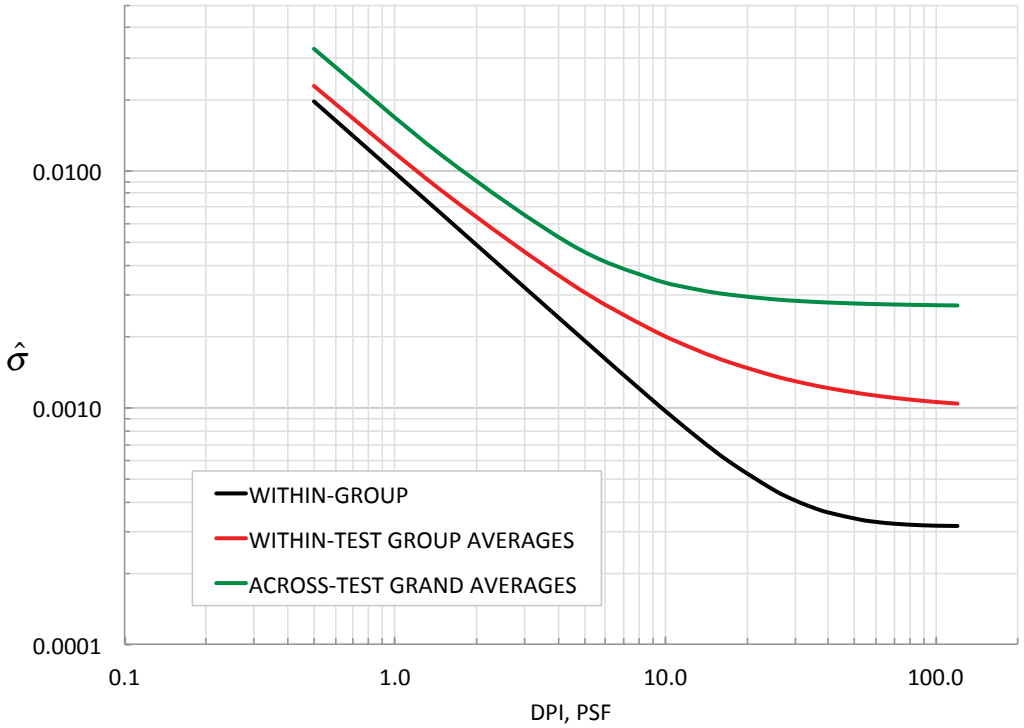

Figure 7. Comparison of the $\hat{\sigma}$ models for C' for the three time frames of variation; 14x22 CSP.

Figure 8. 14x22 check standard model (CSM).

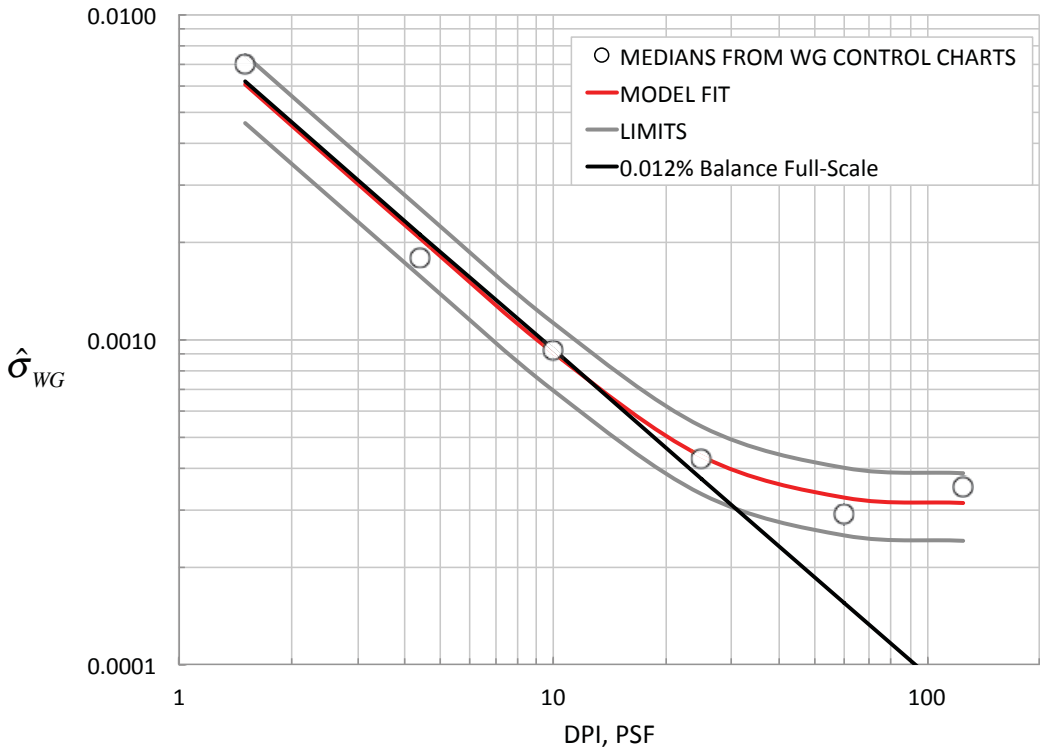

Figure 9. Model of $\hat{\sigma}_{WG}$ for C_N with control limits for 82 DOF; 14x22 CSM.

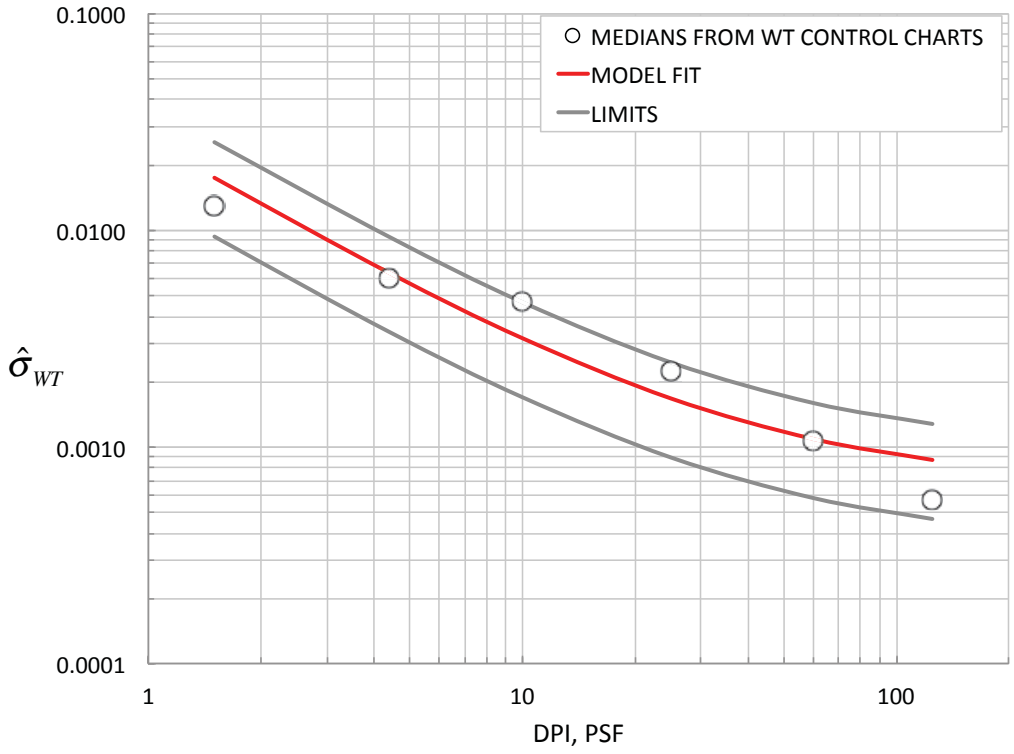

Figure 10. Model of $\hat{\sigma}_{WT}$ for C_N with control limits for 22 DOF; 14x22 CSM.

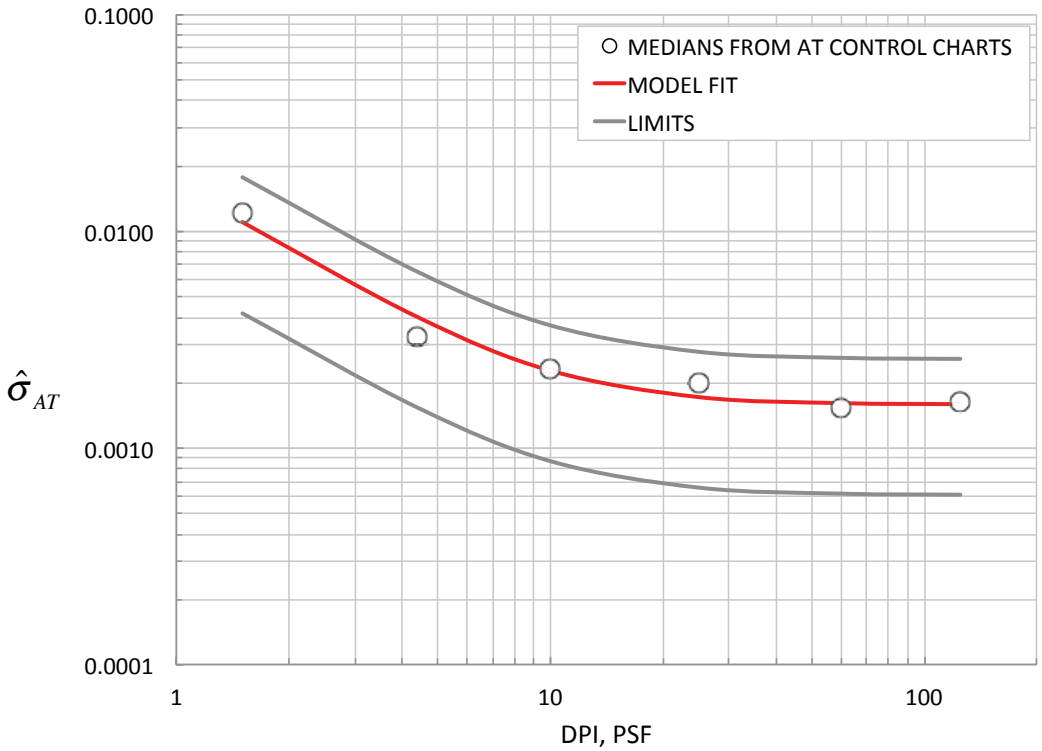

Figure 11. Model of $\hat{\sigma}_{AT}$ for C_N with control limits for 12 DOF; 14x22 CSM.

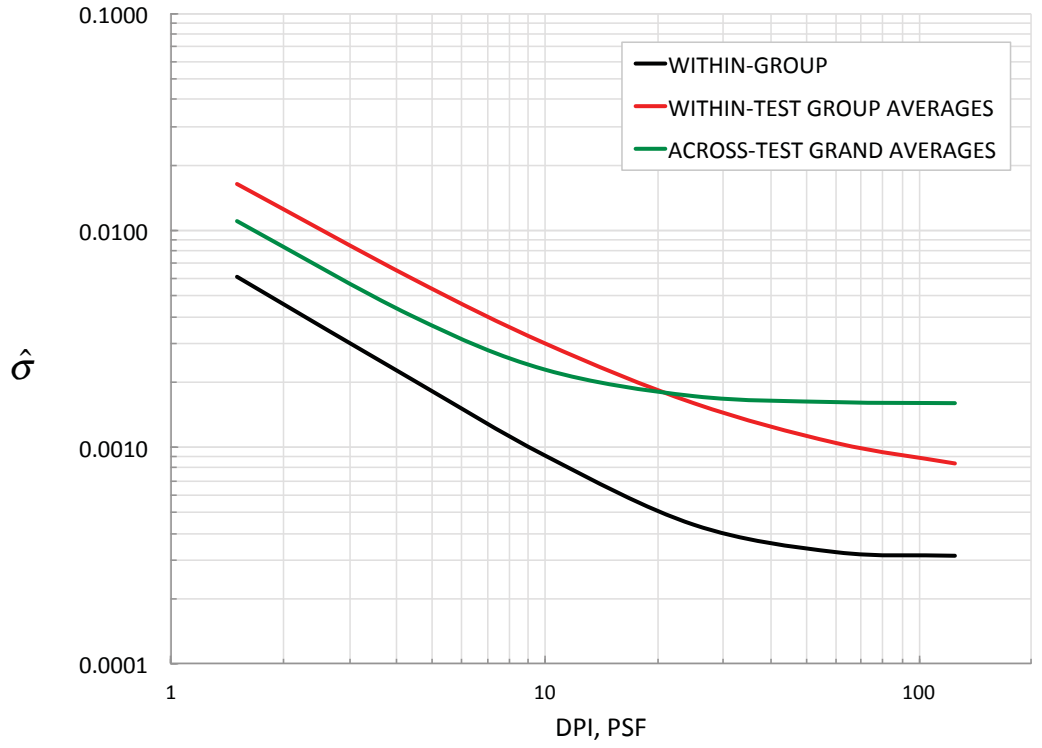

Figure 12. Comparison of the $\hat{\sigma}$ models for C_N for the three time frames of variation; 14x22 CSM.

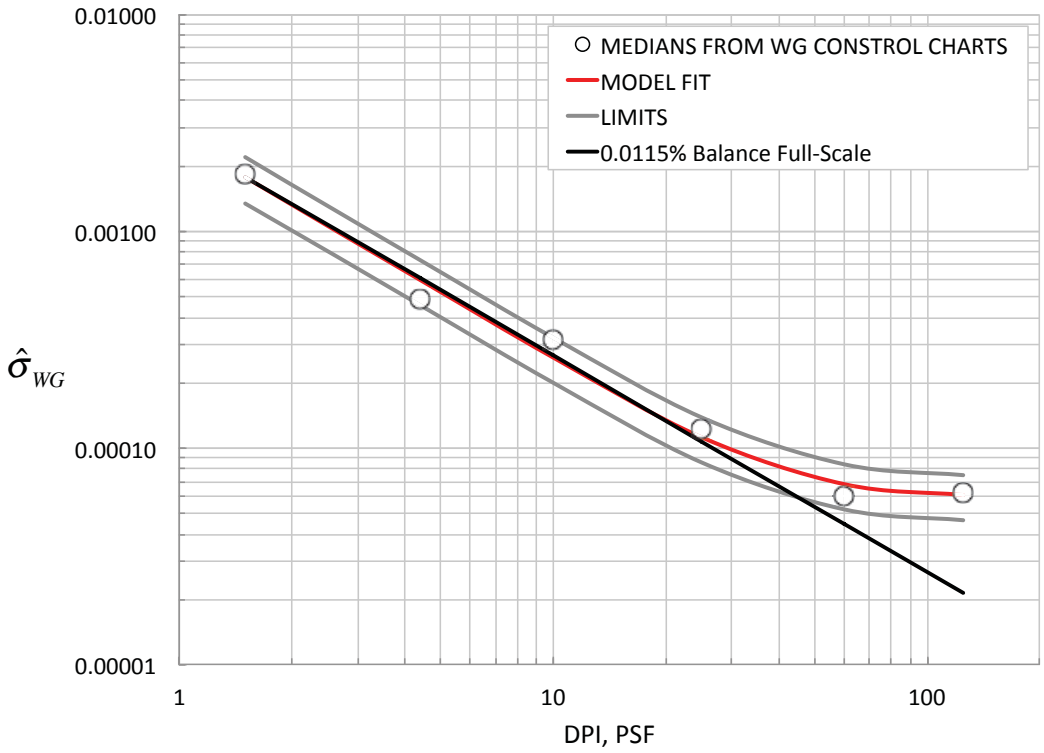

Figure 13. Model of $\hat{\sigma}_{WG}$ for C_A with control limits for 82 DOF; 14x22 CSM.

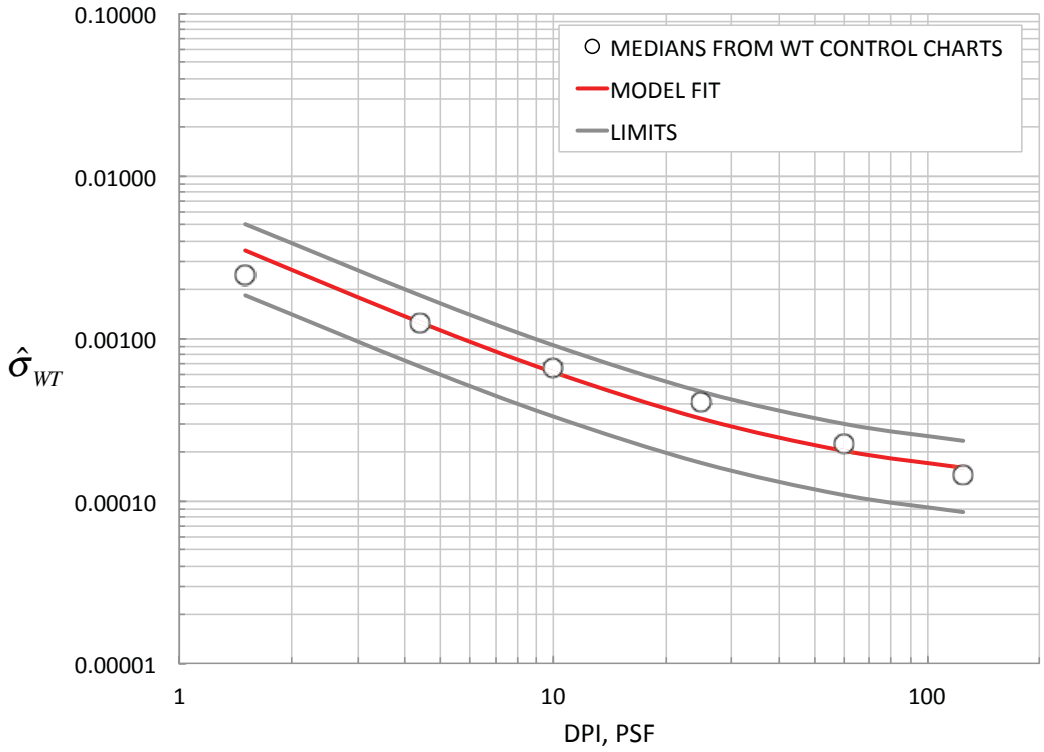

Figure 14. Model of $\hat{\sigma}_{WT}$ for C_A with control limits for 22 DOF; 14x22 CSM.

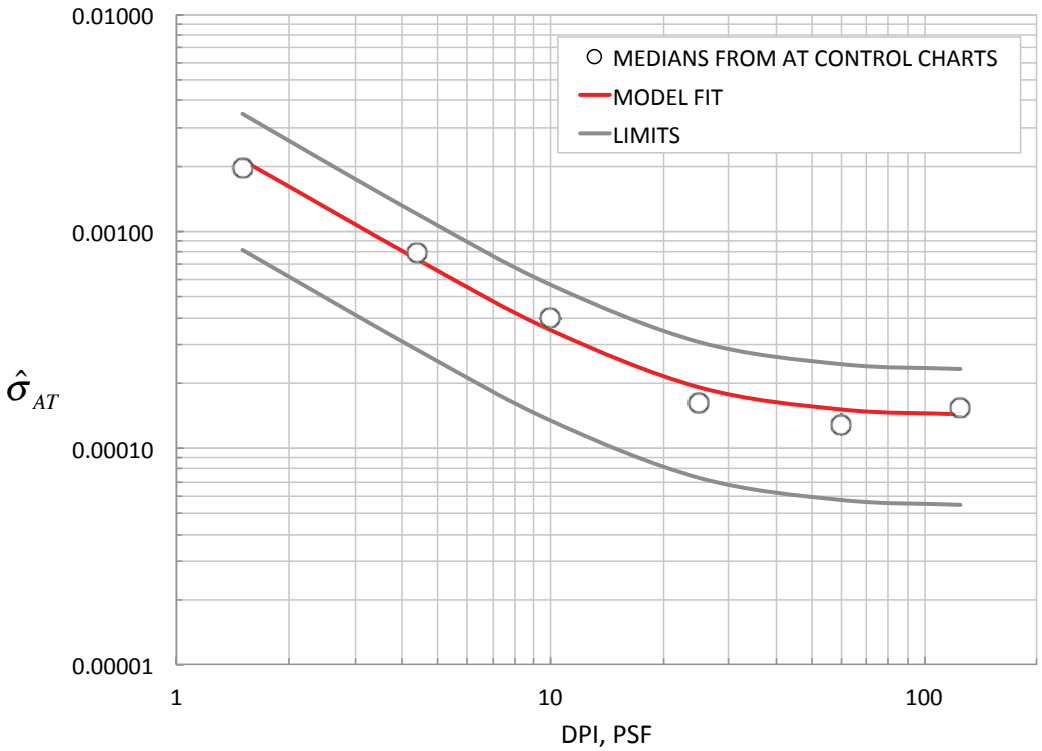

Figure 15. Model of $\hat{\sigma}_{AT}$ for C_A with control limits for 12 DOF; 14x22 CSM.

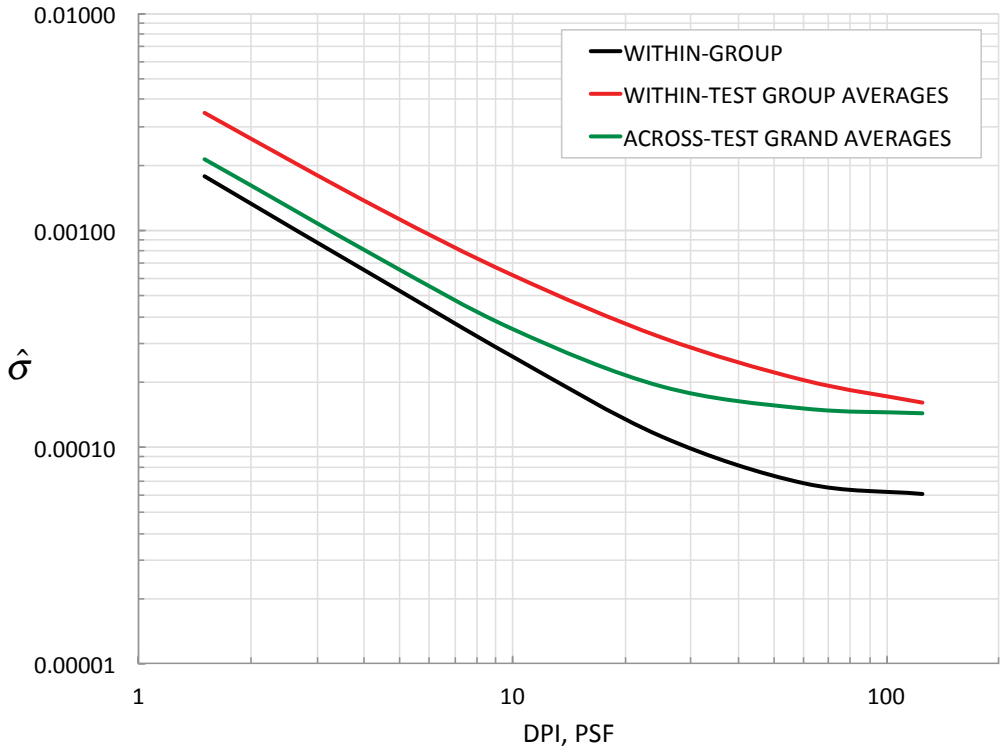

Figure 16. Comparison of the $\hat{\sigma}$ models for C_A for the three time frames of variation; 14x22 CSM.

Figure 17. National Transonic Facility (NTF) check standard model.

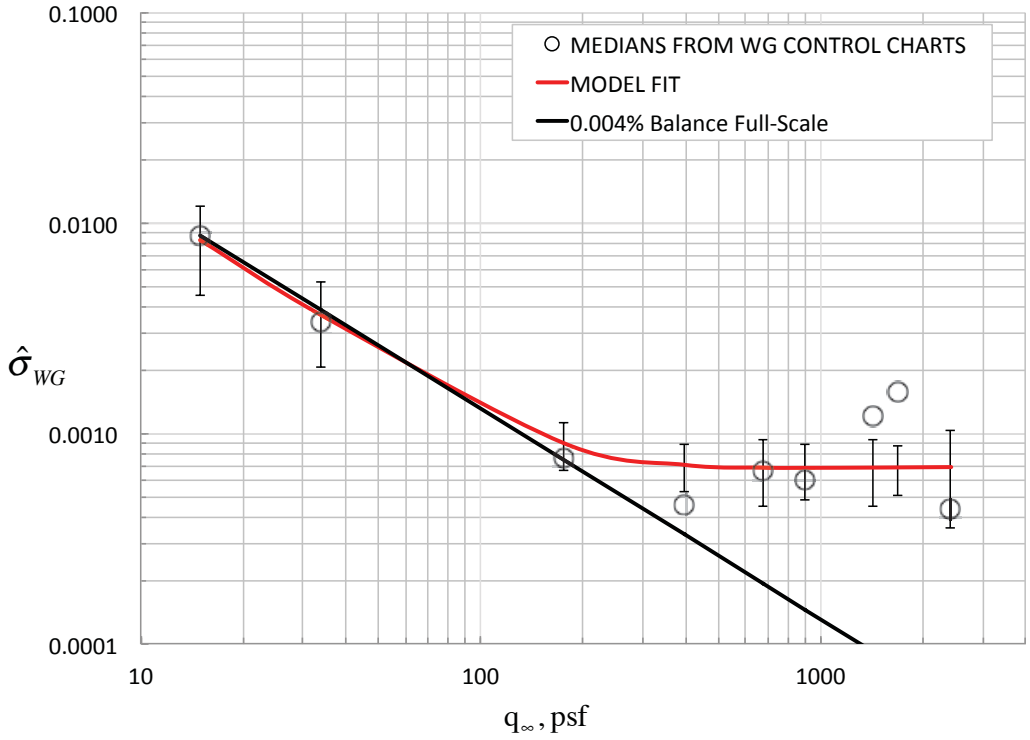

Figure 18. Model of $\hat{\sigma}_{WG}$ for C_N with control limits for various DOF; NTF CSM.

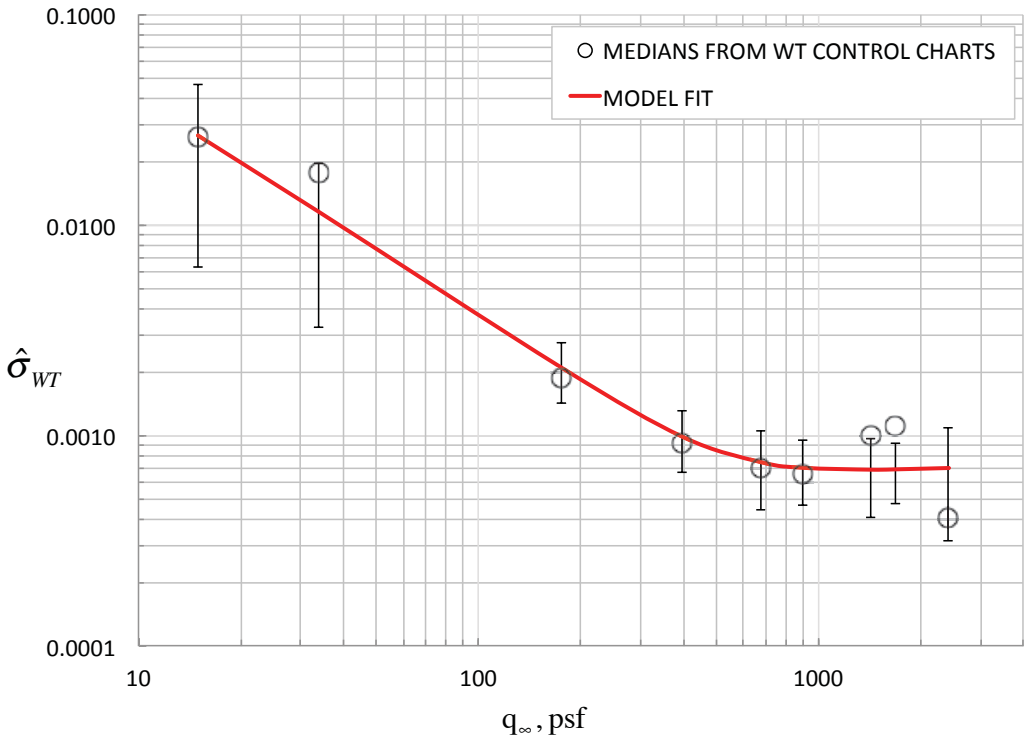

Figure 19. Model of $\hat{\sigma}_{WT}$ for C_N with control limits for various DOF; NTF CSM.

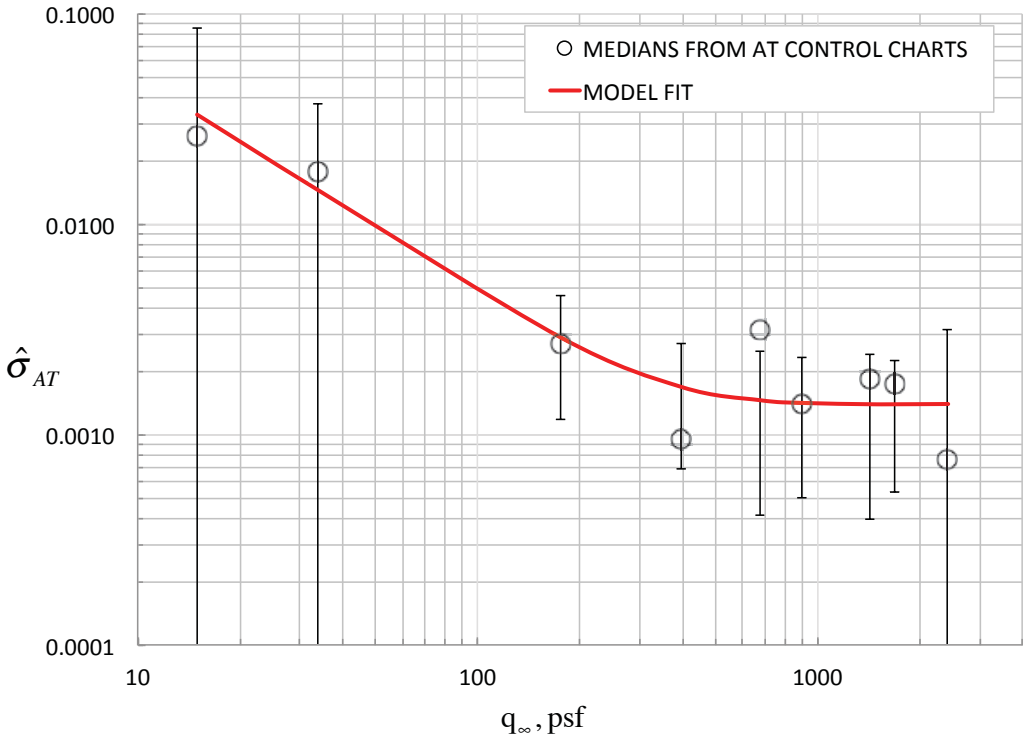

Figure 20. Model of $\hat{\sigma}_{AT}$ for C_N with control limits for various DOF; NTF CSM.

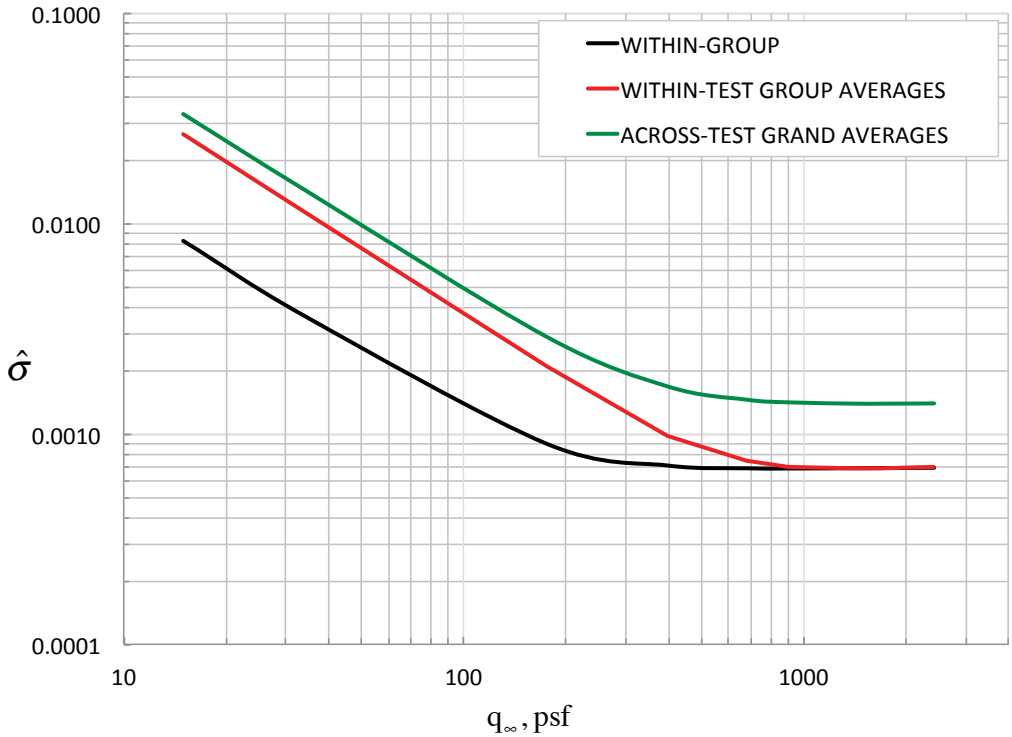

Figure 21. Comparison of the $\hat{\sigma}$ models for C_N for the three time frames of variation; NTF CSM.

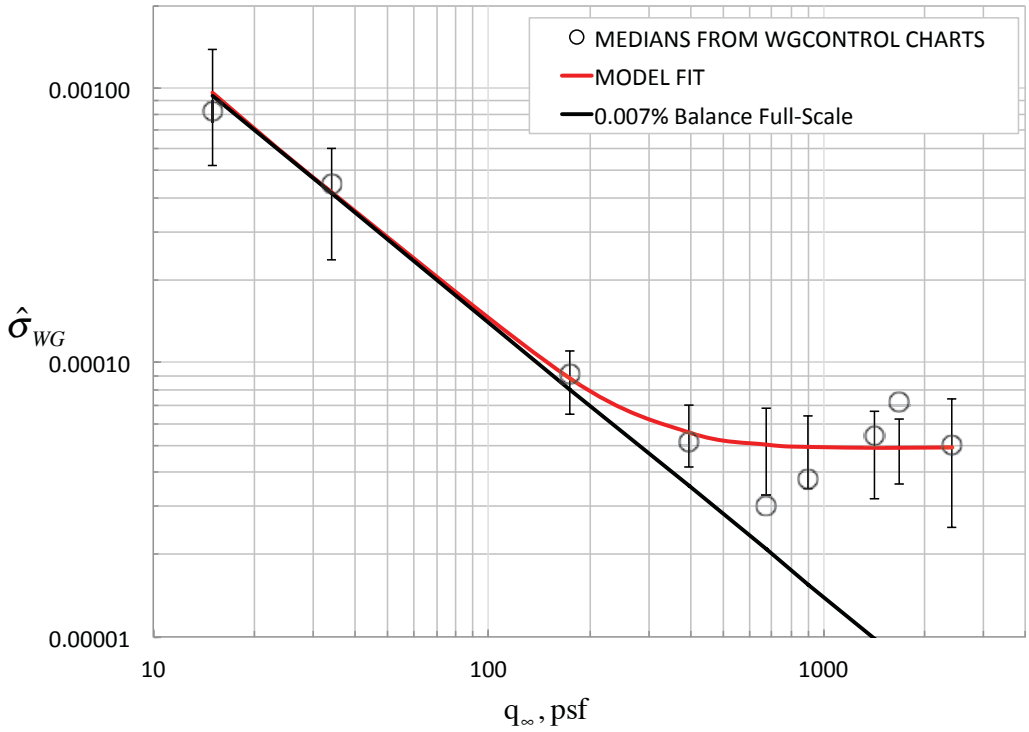

Figure 22. Model of $\hat{\sigma}_{WG}$ for C_A with control limits for various DOF; NTF CSM.

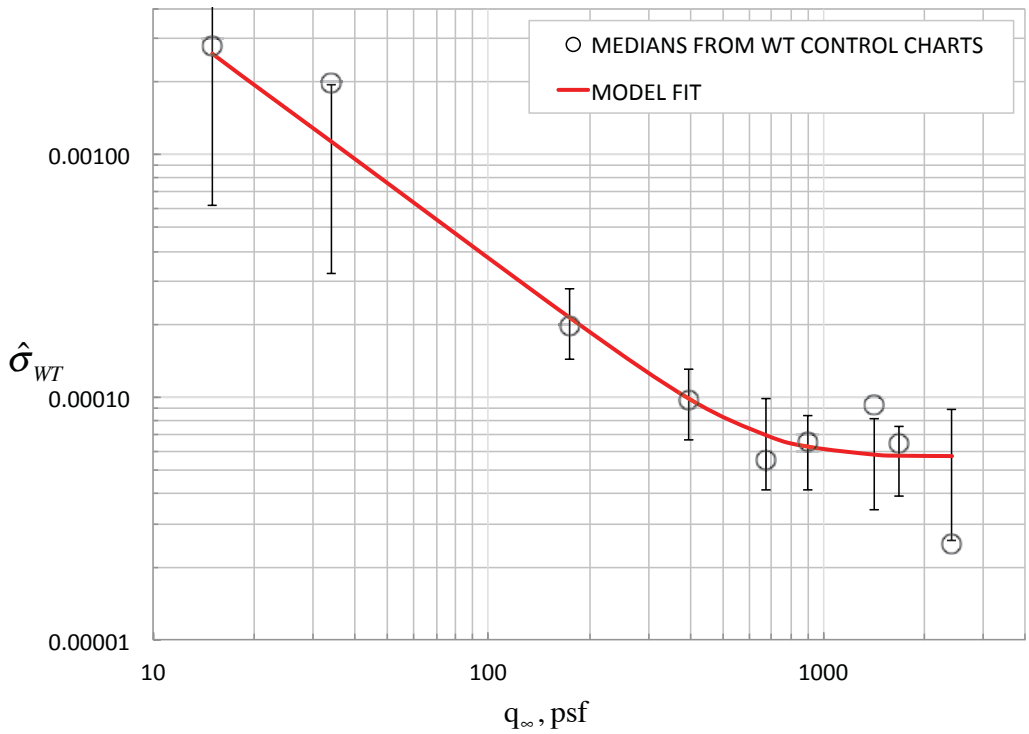

Figure 23. Model of $\hat{\sigma}_{WT}$ for C_A with control limits for various DOF; NTF CSM.

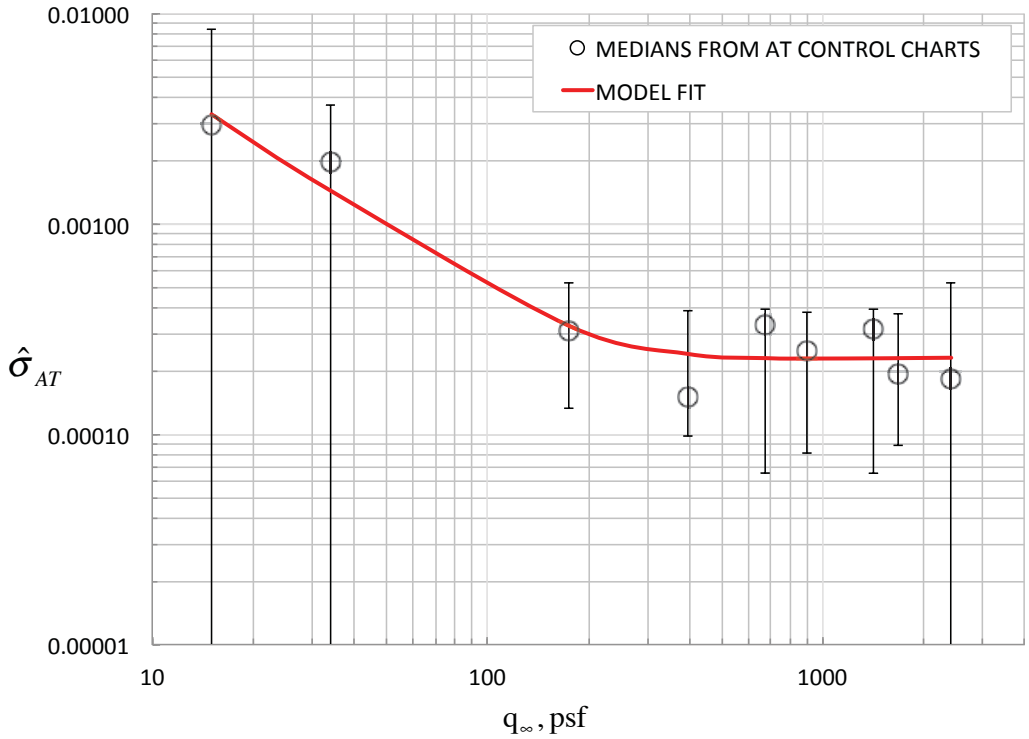

Figure 24. Model of $\hat{\sigma}_{AT}$ for C_A with control limits for various DOF; NTF CSM.

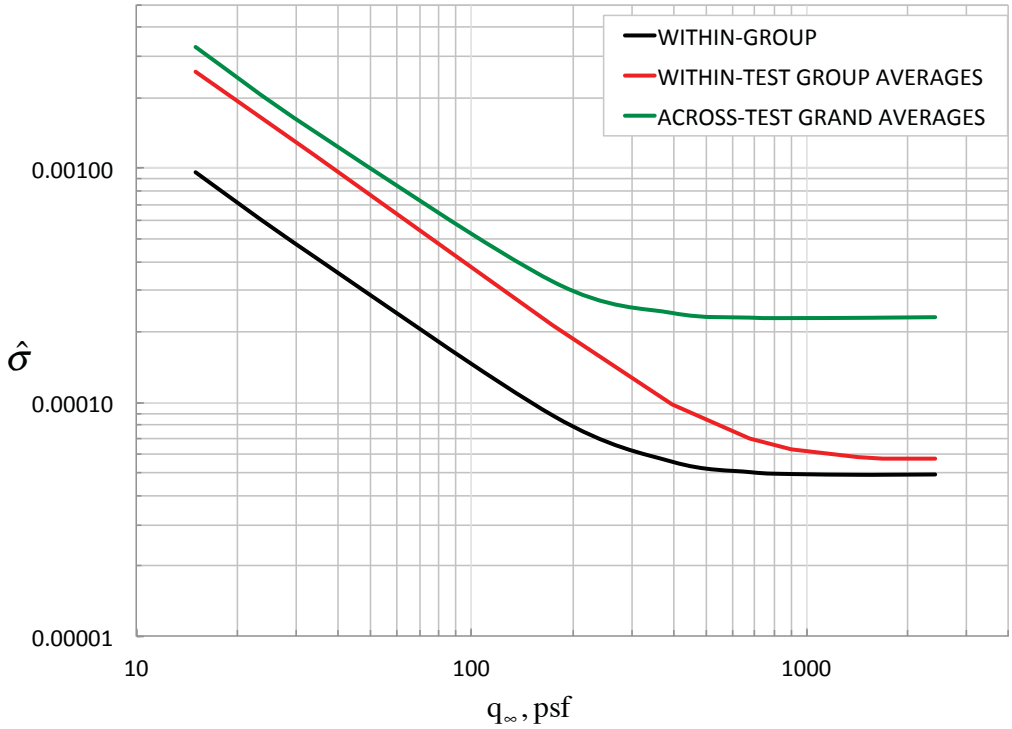

Figure 25. Comparison of the $\hat{\sigma}$ models for C_A for the three time frames of variation; NTF CSM.

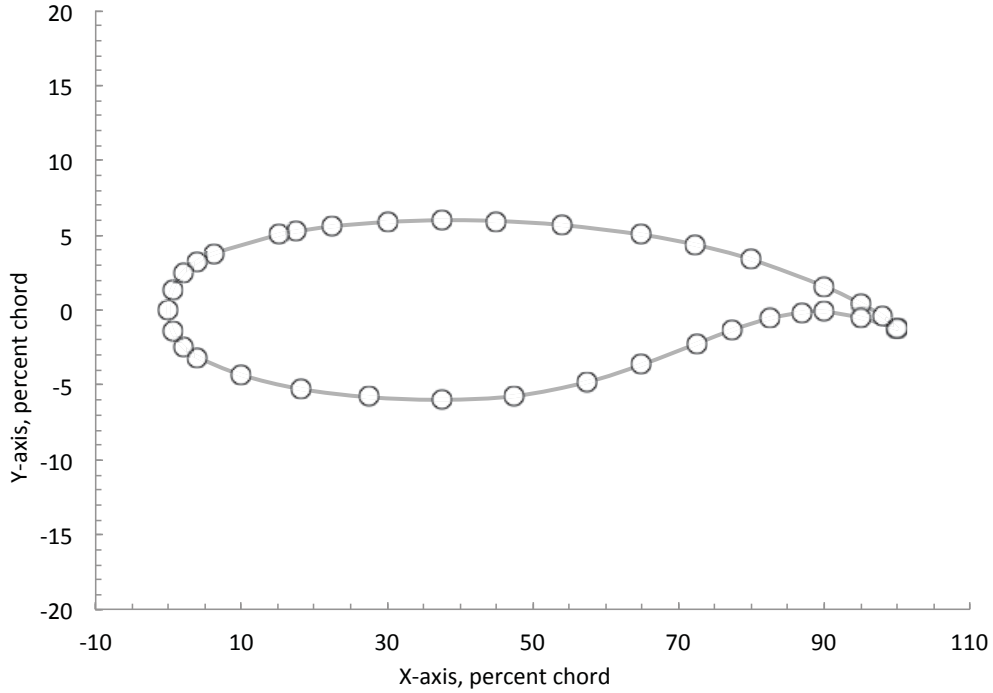

Figure 26. Airfoil and pressure tap locations for the LTPT check standard model.

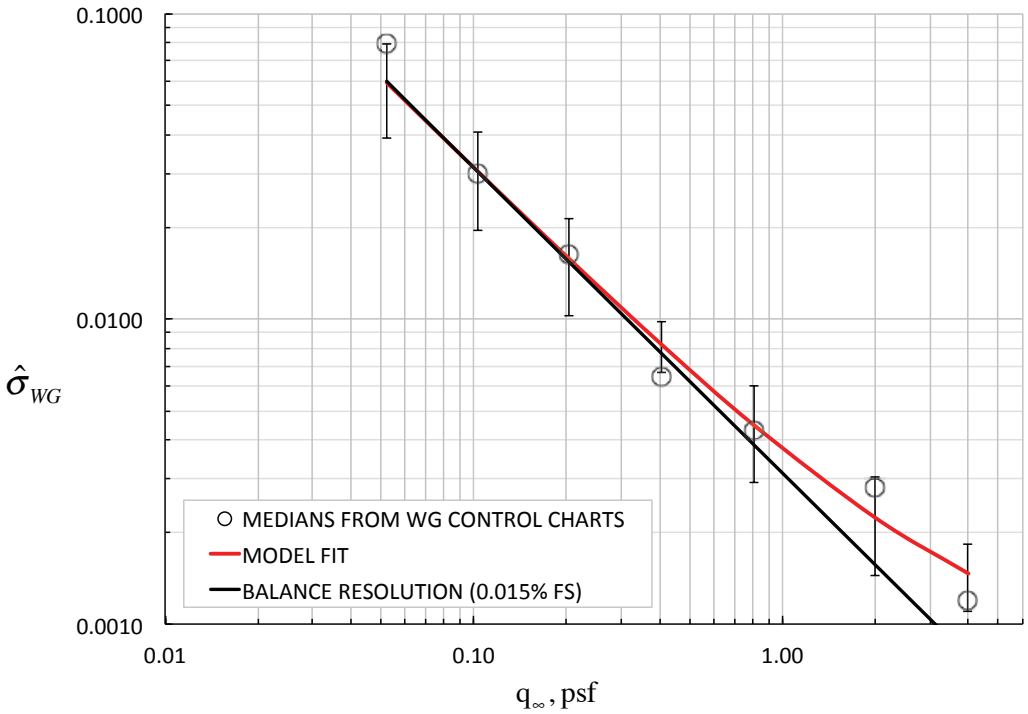

Figure 27. Model of $\hat{\sigma}_{WG}$ for balance C_L with control limits for various DOF; LTPT CSM (10 back-to-back polars in each group).

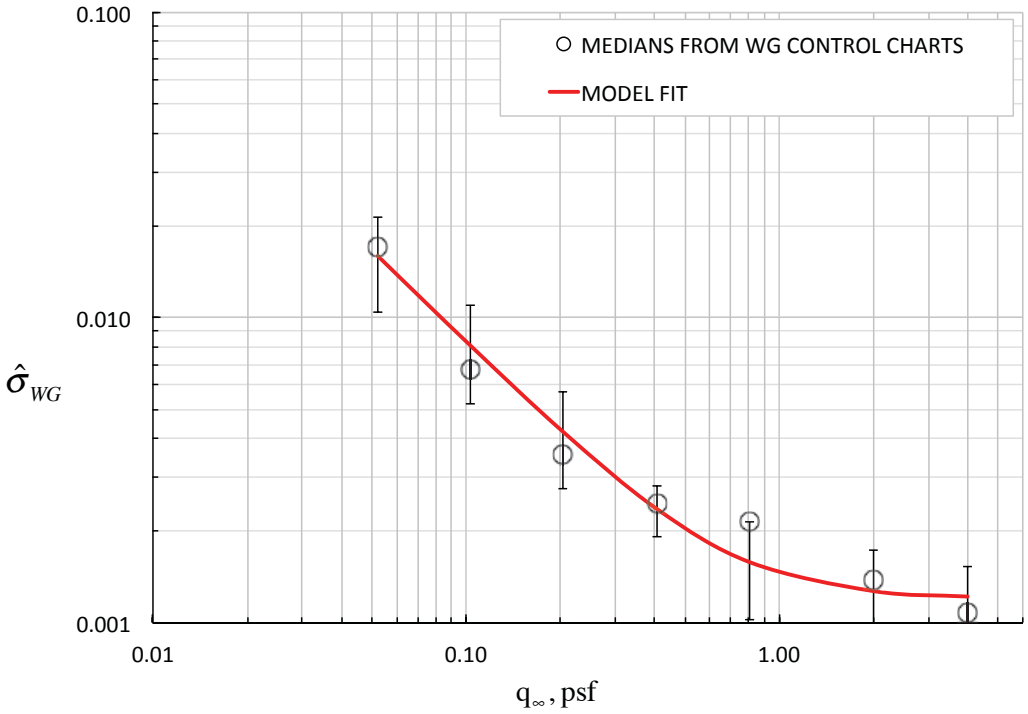

Figure 28. Model of $\hat{\sigma}_{WG}$ for pressure C_L with control limits for various DOF; LTPT CSM (10 back-to-back polars in each group).